EXPLOITATION OF BURST OVERLAPPING AREAS OF TOPS DATA. APPLICATION TO SENTINEL-1

Nestor Yague-Martinez, Pau Prats-Iraola, Muriel Pinheiro and Marc Jaeger

German Aerospace Center (DLR), Microwaves and Radar Institute, Germany

ABSTRACT

This contribution will present the investigations carried out with stacked time-series of TOPS acquisitions to retrieve azimuth displacements. The exploitation of the burst overlapping areas allows to retrieve highly accurate ground displacement estimates in that direction, mitigating the limited performance of classical correlation techniques, due to the low resolution of the mode. The focus of this contribution is the application to time-series of Sentinel-1 data, where slow azimuthal motion is expected. Results with Sentinel-1 data on the proposed methodology are provided for the region of Balochistan, in Pakistan.

Index Terms— Synthetic aperture radar, interferometry, TOPS, Sentinel-1, overlaps, ESD, time series, azimuth deformation.

1. INTRODUCTION

The use of cross-correlation techniques to obtain sensitivity in the along-track direction, traditionally used with StripMap images [1], does not provide enough accuracy for TOPS mode since its performance depends on the azimuth resolution, lower for TOPS than for StripMap. This contribution explores an alternative consisting on the use of spectral diversity techniques [2] applied to the overlap regions between bursts. The explotation of these areas has also been applied to image pairs with Sentinel-1, e.g., in [3]. In [4] the multi-look acquisition principle of ALOS-2 ScanSAR data is exploited following the same principle but obtaining a continuous coverage. The use of a dedicated 2-looks mode for azimuth shift measurement was already proposed and demonstrated with TerraSAR-X in 2015 [5] and time-series results provided after two years in [6]. In this contribution we focus on the the retrieval of azimuth ground displacements with Sentinel-1 data from the overlapping areas and apply to time-series. The limited coverage of the estimates implies a discontinuous azimuth deformation mapping, however very valuable for certain scenarios, where smooth large-scale behavior is expected, allowing an interpolation on the regions between overlaps. A performance analysis is provided in section 2. In section 4 results with Sentinel-1 data over a region in Pakistan affected by post-seismic displacement are provided.

2. PERFORMANCE

The spectral separation for a target on ground observed by two consecutive bursts can be exploited to retrieve an accurate estimation of the azimuthal motion. From an interferometric pair, two interferograms can be generated over the overlapping areas. The phase of the differential interferogram, ϕ_{ESD}, is proportional to the azimuth shift, according to [2]:

$$\phi_{\mathrm{ESD}}(r,x) = 2\pi \cdot \Delta f_{\mathrm{d}}(r) \cdot \Delta t(r,x), \tag{1}$$

where $\Delta f_{\mathrm{d}}(r)$ is the spectral separation between both observations at the overlapping areas for a given range, r. The spectral separation is independent of the targets azimuth position. $\Delta t(r,x)$ is the local azimuth misregistration (in temporal units) intended to be measured. The subscript ESD stands for Enhanced Spectral Diversity [7].

The achievable accuracy for the azimuth shift retrieval (in spatial units) is given by:

$$\sigma_{\Delta x} = \frac{\sigma_{\phi_{\mathrm{ESD}}}}{2\pi\Delta f_{\mathrm{d}}} v_{\mathrm{g}} = \frac{1}{2\pi\Delta f_{\mathrm{d}}\sqrt{N}} \frac{\sqrt{1-\gamma^2}}{\gamma} v_{\mathrm{g}}, \tag{2}$$

where $\sigma_{\phi_{\mathrm{ESD}}}$ is the standard deviation of the ESD phase, N is the number of averaged samples, γ the interferometric coherence and v_{g} the beam ground velocity. Establishing a fixed output posting of 200 m in azimuth we obtain the performance curves of Fig. 1 for the retrieval of the along-track ground displacement for TOPS exploiting the overlapping areas and exploiting cross-correlation and for StripMap (for reference). The Sentinel-1 system has been assumed.

As it can be seen, applying cross-correlation to Sentinel-1 images presents a lower accuracy than StripMap due to the lower resolution of the former. We can define the relative performance with respect to StripMap as:

$$\rho_{\mathrm{x\,vs\,SM}} = 10 \cdot \log_{10} \frac{\sigma^2}{\sigma^2_{\mathrm{SM}}} = 10 \cdot \log_{10} \frac{(\Delta f_d^{\mathrm{SM}})^2 \cdot B^{\mathrm{SM}}}{\Delta f_{\mathrm{d}}^2 \cdot B}, \tag{3}$$

where Δf_{d} is the spectral separation and B the target bandwidth; the superindex SM refers to the StripMap mode. Table 1 summarizes the spectral separation and available bandwidth for each approach along with the relative performance

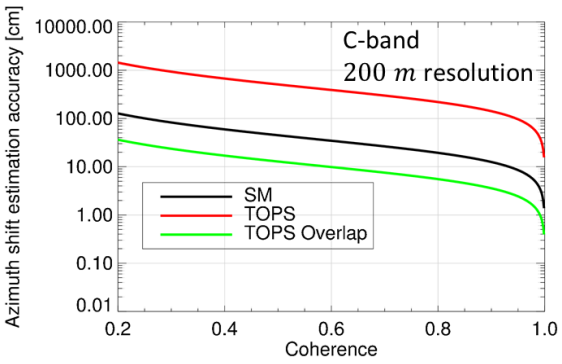

Fig. 1: Along-track ground displacement performance achievable by the different modes for a fixed posting of 200 m with the Sentinel-1 system.

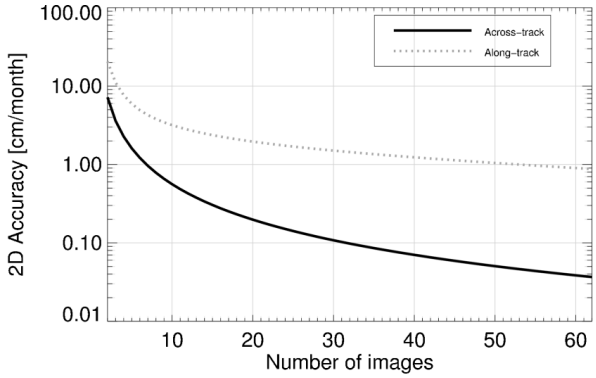

Fig. 2: Achievable mean ground velocity displacement performance in along- and across-track by evaluating the overlapping areas when working with time-series. The Sentinel-1 system has been assumed. An exponential decorrelation model has been used with a time constant of 40 days, a long-term coherence equal to 0.1 and a standard deviation of the turbulent troposphere equal to 1 cm. The number of looks is 200.

with respect to StripMap. Observe the large spectral separation achievable at the overlapping areas between consecutive bursts of the same subswath, which represents a gain on the along-track ground motion retrieval of about 10 dB with respect to StripMap and more than 30 dB with respect to TOPS.

Table 1: Spectral separation and available bandwidth and relative performance with respect to StripMap for each mode

Mode	B[Hz]	Δf_{d} [Hz]	$\rho_{\mathrm{x\,vs\,SM}}$ [dB]
StripMap	1580	1057	0
TOPS	315	210	-21.05
TOPS @ overlaps	315	4800	10.89

In case of working with time series, we obtain the performance curves of the mean velocities shown in Fig. 2 for the along and across directions depending on the number of images employed. An exponential decorrelation model has been used with a time constant of 40 days, a long-term coherence equal to 0.1 and a standard deviation of the turbulent troposphere equal to 1 cm. The number of looks is 200.

We can see that the performances between across and along-track are closer for short stacks. The reason is that the along-track measurement is much less affected by turbulent troposphere, due to its high spatial correlation between looks, as analyzed in [8]. When we have just a few images, the across-track measurement is more affected by the troposphere, since it cannot be estimated properly. Adding more images to the stack enhances the estimation in the across-track direction since the troposphere can be better compensated, whereas the along-track direction improves only due to having more images, however the temporal decorrelation dominates.

3. METHODOLOGY

Our starting point is a stack of images coarsely coregistered where orbital/timing azimuth errors have been corrected. The Enhanced Spectral Diversity (ESD) phases can be computed between each slave image, s^j, and a common master, m, at the overlapping areas between bursts according to:

$$\phi^j_{\mathrm{ESD}} = \arg\left\{(m_i \cdot s_i^{j*}) \cdot (m_{i+1} \cdot s_{i+1}^{j*})^*\right\} \text{@ overlaps}, \quad (4)$$

where m_{i} and s_{i} refer to the i^{th} master and slave complex bursts, respectively, and $m_{\mathrm{i+1}}$ and $s_{\mathrm{i+1}}$ refer to the $(i+1)^{\mathrm{th}}$ master and slave bursts. The superscript j refers to the slave index. Given a desired output product resolution, spatial multilooking can be applied to the InSAR phases / ESD phase. A small multilooking of the interferograms prior to the calculation of the differential interferogram (so-called early-multilooking) increases the estimation efficiency [9].

The estimation of the mean azimuth velocity, v_a, can be done applying the periodogram to the ESD phases of the time-series:

$$\widehat{v_{\mathrm{a}}} = \arg\max_{v_{\mathrm{a}}} \left[\Re\left\{ \sum_i e^{j(\phi_{\mathrm{ESD}}[i] - 2\pi \Delta f_{\mathrm{d}} v_{\mathrm{a}} T[i] v_g[i])} \right\} \right], \quad (5)$$

where $\arg\max_{v_{\mathrm{a}}}\{\cdot\}$ stands for the argument of the maximum (mean azimuth velocity, v_{a}, for which the function attains its largest value). $\phi_{\mathrm{ESD}}[i]$ is the temporal array of ESD phases of each (master-slave) interferogram, i, for each multilooked pixel, Δf_{d} is the Doppler spectral separation between looks for each pixel, and $T[i]$ are the temporal baselines of each

interferogram. Note that the dependency of Δf_{d} and v_{g} with range and azimuth have been omitted for simplicity. We have assumed that the ESD phases are not affected by tropospheric noise as justified in section 2.

4. APPLICATION TO SENTINEL-1 DATA

The methodology described in Section 3 has been applied to two stacks of images in ascending and descending geometry over Balochistan, in Pakistan. This area was affected by strong Earthquakes in November 2013, which could be mapped by different SAR sensors, for instance with TerraSAR-X [10]. After the strong Earthquakes the area experimented post-seismic displacement. Sentinel-1 images were available over the area starting at the end of 2014.

The ascending Sentinel-1 IW dataset has 50 acquisitions and covers a time span of approximately 3 years, from 25 October 2014 until 27 September 2017. The master image has been selected on 23 May 2016. Two slices have been processed being the coverage 250 x 340 km approximately. The top part of Fig. 3 shows a Google Earth representation over the site for the ascending geometry. A TerraSAR-X ScanSAR co-seismic interferogram, covering 100 km in across-track can be seen in the background, showing fringes due to the ground displacement of the 2013 Earthquakes. The 2013 surface rupture line, depicted in orange, has been provided by Ken Hudnut from Caltech employing Landsat pixel offsets. We can observe a smooth spatial variation of the displacement, thus an interpolation can be performed for further analysis. The measured mean azimuth velocity at the overlapping regions is interpolated via an iterative Euler-Lagrange energy minimization scheme [11] and is displayed at the right part. In this figure we can appreciate that the deformation pattern matches the 2013 surface rupture line.

The descending Sentinel-1 IW dataset has 50 acquisitions and covers also a time span of approximately 3 years, from 16 October 2014 until 13 August 2017. The master image has been selected on 27 March 2016. Two slices have been processed delivering the same coverage as for the ascending geometry. The bottom part of Fig. 3 shows the descending results. The mean along-track velocity results from Sentinel-1 are overlaid and displayed on the left. The right part shows the overlay of the interpolated map applying the same procedure as mentioned above. The deformation pattern matches also the 2013 surface rupture line.

5. CONCLUSIONS

The exploitation of the burst overlapping areas of the TOPS acquisition mode represents an opportunity to obtain highly accurate estimates of along-track ground displacements and mitigates this way the low performance of applying correlation techniques given the low azimuth resolution of the mode. The coverage of the estimation is restricted to the overlap regions making it suitable for the study of large scale phenomena, e.g., earthquakes and glacier monitoring. The along-track estimation complements the line-of-sight deformation measurement and aids to the computation of a more homogeneous 3D deformation retrieval, which can be of valuable interest for geophysical applications. We have applied this procedure to two 3-years stacks of Sentinel-1 images, in ascending and descending geometry, over Balochistan, Pakistan. This area experiments post-seismic deformation after strong Earthquakes that took place in 2013. The mean azimuth velocity has been retrieved for both of them revealing a deformation signal which matches the 2013 surface rupture line. An interpolation of the mean velocity map employing an iterative Euler-Lagrange energy minimization scheme shows the potential of the procedure to map large scale deformation phenomena.

6. REFERENCES

[1] R. Michel, J. P. Avouac, and J. Taboury, "Measuring ground displacements from SAR amplitude images: Application to the Landers earthquake," *Geophys. Res. Lett., 26(7), 875878.*, 1999.

[2] R. Scheiber and A. Moreira, "Coregistration of interferometric SAR images using spectral diversity," *Geoscience and Remote Sensing, IEEE Transactions on*, vol. 38, no. 5, pp. 2179–2191, Sep 2000.

[3] A. Hooper and K. Spaans, "Sentinel-1 along -track InSAR for global strain rate estimation," in *FRINGE 2017*, http://fringe.esa.int/files/presentation523.pdf.

[4] C. Liang and E. J. Fielding, "Measuring Azimuth Deformation With L-Band ALOS-2 ScanSAR Interferometry," *IEEE Transactions on Geoscience and Remote Sensing*, vol. 55, no. 5, pp. 2725–2738, May 2017.

[5] P. Prats-Iraola, M. Rodriguez-Cassola, N. Yague-Martinez, P. Lopez-Dekker, R. Scheiber, F. De Zan, T. Kraus, and S. Wollstadt, "Repeat-pass interferometric experiments with the TanDEM-X constellation for accurate along-track motion estimation," in *2015 IEEE International Geoscience and Remote Sensing Symposium (IGARSS)*, July 2015, pp. 4077–4080.

[6] N. Yague-Martinez, P. Prats-Iraola, and S. Wollstadt, "Time-Series Evaluation Of Azimuth Displacements With The Experimental TerraSAR-X 2-Looks TOPS Acquisition Mode," in *FRINGE 2017*, http://fringe.esa.int/files/presentation175.pdf.

[7] P. Prats-Iraola, R. Scheiber, L. Marotti, S. Wollstadt, and A. Reigber, "TOPS Interferometry with TerraSAR-X," *Geoscience and Remote Sensing, IEEE Transactions on*, vol. 50, no. 8, pp. 3179–3188, Aug 2012.

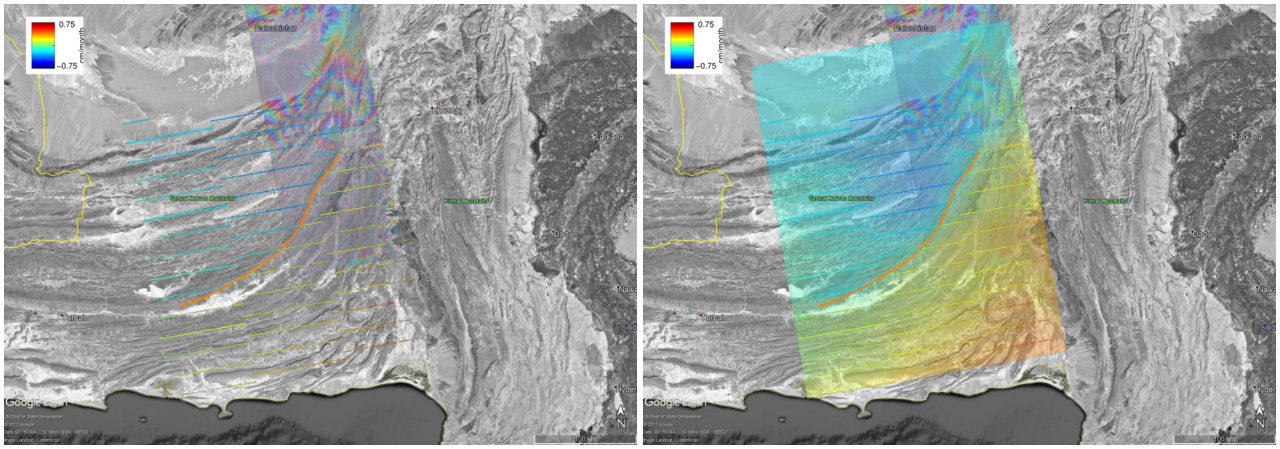

(a) Ascending

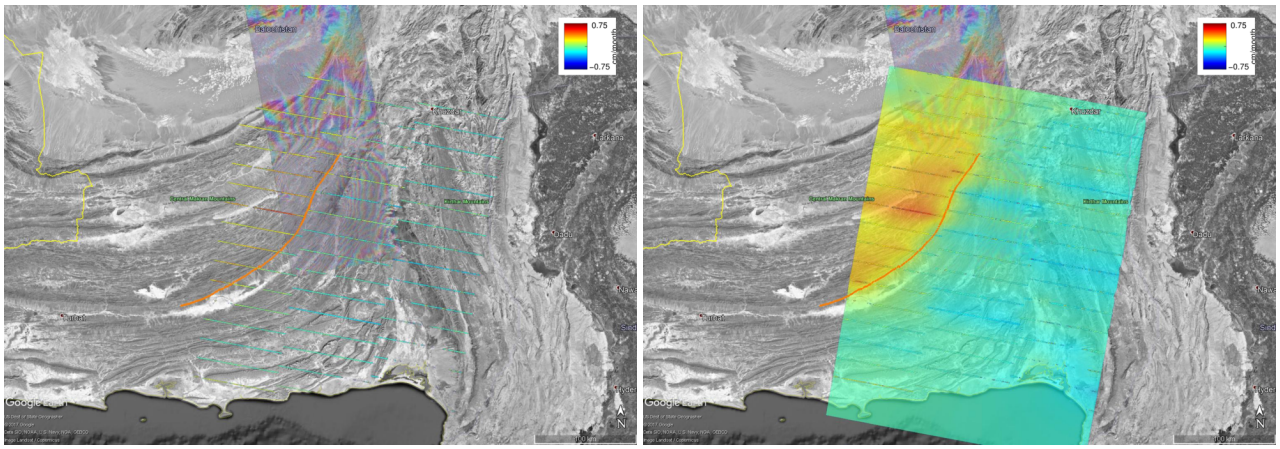

(b) Descending

Fig. 3: (Left) mean ground velocity in along-track direction evaluated at the overlapping areas between bursts of the same subswath. A TerraSAR-X ScanSAR co-seismic interferogram is also displayed in the background showing fringes due to the 2013 Earthquakes. The 2013 surface rupture line is depicted in orange. (Right) interpolated mean azimuth velocity via an iterative Euler-Lagrange energy minimization procedure. The results of ascending and descending geometries are displayed on the top and bottom, respectively.

[8] P. Prats-Iraola, P. Lopez-Dekker, F. De Zan, N. Yagüe-Martínez, M. Zonno, and M. Rodriguez-Cassola, "Performance of 3-D Surface Deformation Estimation for Simultaneous Squinted SAR Acquisitions," *IEEE Transactions on Geoscience and Remote Sensing*, vol. PP, no. 99, pp. 1–12, 2017.

[9] F. De Zan, P. Prats-Iraola, and M. Rodriguez-Cassola, "On the Dependence of Delta-k Efficiency on Multi-looking," *IEEE Geoscience and Remote Sensing Letters*, vol. 12, no. 8, pp. 1745–1749, Aug 2015.

[10] N. Yague-Martinez, P. Prats-Iraola, F. Rodriguez Gonzalez, R. Brcic, R. Shau, D. Geudtner, M. Eineder, and R. Bamler, "Interferometric Processing of Sentinel-1 TOPS Data," *IEEE Transactions on Geoscience and Remote Sensing*, vol. 54, no. 4, pp. 2220–2234, April 2016.

[11] Beg M.F., Miller M., Trouvé A., and Younes L., "The Euler-Lagrange Equation for Interpolating Sequence of Landmark Datasets," *Ellis R.E., Peters T.M. (eds) Medical Image Computing and Computer-Assisted Intervention. MICCAI 2003. Lecture Notes in Computer Science, vol 2879. Springer, Berlin, Heidelberg*, 2003.